PHYSICS AND CHEMISTRY OF SOLID STATE
V.21, No.2 (2020) pp. 325-331

Vasyl Stefanyk Precarpathian National University

ФІЗИКА І ХІМІЯ ТВЕРДОГО ТІЛА
Т. 21, № 2 (2020) С. 325-331

DOI: 10.15330/pcss.21.2.325-331

UDC 544.77.023.522:543.456:548.75 ISSN 1729-4428

I.F. Mironyuk[1], V.O. Kotsyubynsky[1], T.V. Dmytrotsa[2], L.M. Soltys[1], V.M. Gun'ko[3]

Atomic Structure and Morphology of Fumed Silica

[1]*Vasyl Stefanyk Precarpathian National University, Ivano-Frankivsk, Ukraine, myrif555@gmail.com*
[2]*Ivano-Frankivsk National Medical University, Ivano-Frankivsk, Ukraine, t0955386758@gmail.com*
[3]*Chuiko Institute of Surface Chemistry, Kyiv, Ukraine, vlad_gunko@ukr.net*

The comparative analysis of atomic structure and morphology of fumed silica nanoparticles prepared under different synthesis conditions has been carried out using TEM, FTIR, quantum chemistry, and low-temperature nitrogen adsorption methods. It has been determined that the structure of amorphous silica nanoparticles is formed by branched chain-like clusters of 0.6 - 2.4 nm in size that correspond to proto-particles or nuclei of nanoparticles. A linear part of the smallest clusters is consisted of two tetrahedra SiO_4 with common oxygen atom and oppositely directed vertices. The inter-tetrahedral average angle Si – O – Si is ca. 180˚. It has been shown that the textural porosity of fumed silica powder depends on the initial degree of aggregation of nanoparticles. The average mesopores (1 nm < R < 25 nm) volume is in the rage of 0.26 - 0.60 $cm^3 \cdot g^{-1}$ for materials pretreated at different temperatures. It has been found out that the mean pores radius decreases from 34 nm to 10 nm with decreasing average size of silica nanoparticles. The micropores (R < 1 nm) contribution to the total pore volume is small for all materials (0.003 - 0.029 $cm^3 \cdot g^{-1}$).

Keywords: fumed silica, crystalline silica, silica clusters, siloxane bond.

Received 27 March 2020; Accepted 15 June 2020.

Introduction

The main feature both of natural and synthetic forms of disordered amorphous silica is the absence of long-range ordering of the oxygen and silicon atoms arrangement, the isotropy of physical and chemical properties, and the difference from zero of the entropy of these materials at 0 K. The structure of quartz glass formed by three-dimensional disordered grid consisted of vertices-joined [SiO_4] tetrahedra has been well investigated [1]. The radial distribution function of quartz glass has the first intense maximum at ca. 0.162 nm and the second one at about 0.265 nm [2]. These distances correspond to the Si–O and O–O bond lengths in [SiO_4] tetrahedra and are close to similar characteristics of the structure of crystalline silica form with tetrahedral coordination of silicon atoms [3]. The blurred character of subsequent maxima indicates short-range ordering (0.6 - 0.7 nm) for quartz glass and other amorphous forms of silica. Most models of amorphous silica are based on the disordered spatial grid approach [4]. At the same time, the presence of local ordering in the X-ray amorphous silica is possible at the distance up to 0.8 - 1.0 nm [5]. There are some notifications about crystal-like structural motives in disordered silica. There are conclusions on the presence of ultrafine crystallites in amorphous silica of quartz or tridymite structures [6] based on FTIR data. The ribbon-like crystallites with a wollastonite-like structure were observed in silica gel using optical spectroscopy [7]. According to NMR spectroscopy data, the structure of silica gel consists of fragments of cristobalite [8], but for fumed silica both quartz and cristobalite motives were observed [9].

The most forms of disordered silica have a globular morphology at a nano/microscaled level. The nucleation and growth of globular nanoparticles is typical for the pyrogenic synthesis that is caused by flame reaction conditions (reaction medium, flame velocity, turbulence and temperature). Coagulation and coalescence processes are happened simultaneously with primary silica nanoparticles formation that leads to the formation of various aggregates of nonporous nanoparticles (NPNP) and agglomerates of aggregates. The morphological properties of fumed silica depend on temperature of

reaction medium and velocity of gas/vapor flow. The variations of these parameters allow one to control the material structure and texture. At the same time, there is a lack of information on the morphology effect on the short-range ordering in fumed silica nanoparticles. The combination of optical spectroscopy and HRTEM methods may allow us to observe ultrafine clusters in the amorphous silica nanoparticles. The main aim of this work was to study correlations between the short-range structural arrangement and morphological characteristics of fumed silica.

I. Materials and characterization

The fumed silica samples were synthesized by combustion of silicon tetrachloride vapor in a hydrogen-air flame at 1100 – 1400 °C [10]. The morphological characteristics of the powders were analyzed using low-temperature nitrogen adsorption-desorption isotherms recorded using a Micrometrics ASAP 2405N analyzer. The calculation of the BET specific surface area and pore volume were done according to standard methods [11]. The pore size distributions were calculated using modified Nguyen-Do method and a regularization procedure at $\alpha = 0.01$ [12] with a model of pores as voids between nonporous nanoparticles (NPNP) in aggregates and agglomerates. The morphology of silica nanoparticles and their secondary structures was investigated using a transmission electron microscope (TEM) JEM 2100F (accelerating voltage 80 -200 kV, points and lines resolution of ca. 0.19 nm and 0.1 nm, respectively). FTIR spectra were recorded using a Nicolet 8700A (Thermo Scientific) spectrometer at room temperature.

II. Results and discussion

Fumed silica was synthesized as a result of high temperature oxidation of silicon tetrachloride in the oxygen-hydrogen flame at industrial conditions [13]. The properties of fumed silica depend on many factors: a molar ratio of the reagents ($SiCl_4$, O_2, H_2), gas flow velocity and turbulence in a reaction chamber, and flame temperature. The analytical characteristics of the test samples correspond to the specifications of the technical conditions of Ukraine for industrial grades of silica A-50, A-150, A-200, A-300, and A-380 (Technical conditions of Ukraine 24.6-05540209:2007). The formation of fumed silica nanoparticles can be divided into several steps: protoparticles nucleation → primary particles → aggregates → agglomerates [14].

At the first stage of the reaction, the oxidation of silicon tetrachloride molecules, first, to silicon monoxide and, second, to silicon dioxide is occured. Gas-phase polymerization leads to the formation of small oligomeric molecules $(SiO_2)_x$ ($x \geq 6 - 10$) that form protoparticles (Fig. 1) [15, 16] as a kinetically unstable cluster of SiO_2 molecules [17]. The primary particle formation at the next stage is a result of spatial optimization of $[SiO_{4/2}]$ species coordination with the unification of separate oligomeric chains. These processes are accompanied by coalescence of protoparticles, surface energy minimization and leads to mostly spherical morphology of primary particles. These primary particles were directly observed by TEM for A–150 and A–380 samples (Fig. 2). The aggregation of primary particles at the next stage is a result of chemical bonding of surfaces hydroxyl groups with elimination of water and formation of ordinary siloxane bonds [18]. The compactification of primary nanoparticles due to direct sintering with the formation of the secondary particles can associate to mesoporous 3D-grid (Fig. 2). This texture provides the hysteresis loops formation on the adsorption-desorption isotherms of nitrogen (Fig. 3, a). The calculated values of the BET specific surface area for investigated samples are 52, 150, 179, 270, and 414 m^2/g. The average nanoparticle sizes of A-50, A-150, A-200, A-300, and A-380 samples are 50, 18, 15, 10, and 7 nm, respectively. A linear ($R^2 = 0.98$) dependence of the total pore volume vs. specific surface area (Fig. 3, b) is an evidence of a smaller aggregation degree for silicas with a smaller S_{BET} value.

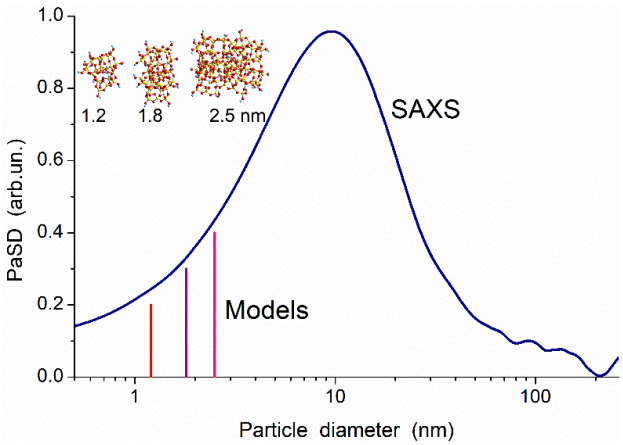

Fig. 1. Particle size distribution for A-300 calculated using small angle X-ray scattering (SAXS) [15] and clusters with 22, 44, and 88 tetrahedrons calculated using DFT method (ωB97X-D/cc-pVDZ, Gaussian 09, D.01) [16].

Mesopores are dominating for all investigated silicas. A decrease in the average particles size causes a decline of mesopore size values (Fig. 3, c) since the samples with the most probable pore size of 7, 10, 15, and 50 nm have the average pore size of 6, 8.5, 10.5, and 34 nm, respectively. The micropores contribution to the total pore volume is respectively low (0.003 - 0.029 $cm^3 \cdot g^{-1}$). The direct HRTEM observation of silica particles allows one to detect nanopores of ca. 0.3 - 0.5 nm in sizes localized along atomic chains and as voids between adjacent NPNP in aggregates. The nanopores content increases with decreasing average particle size because the number of contacts between adjacent smaller NPNP increases in more strongly compacted aggregates.

Its known that the crystalline structures of silica and silicates are based on the $[SiO_4]$ tetrahedrons formed at sp^3 hybridization of the silicon atom valence electrons. According to the Magnus rule, the type of coordination polyhedrons in the oxide material depends on the ratio between of the cation (r_c) and anion (r_a) radii. The

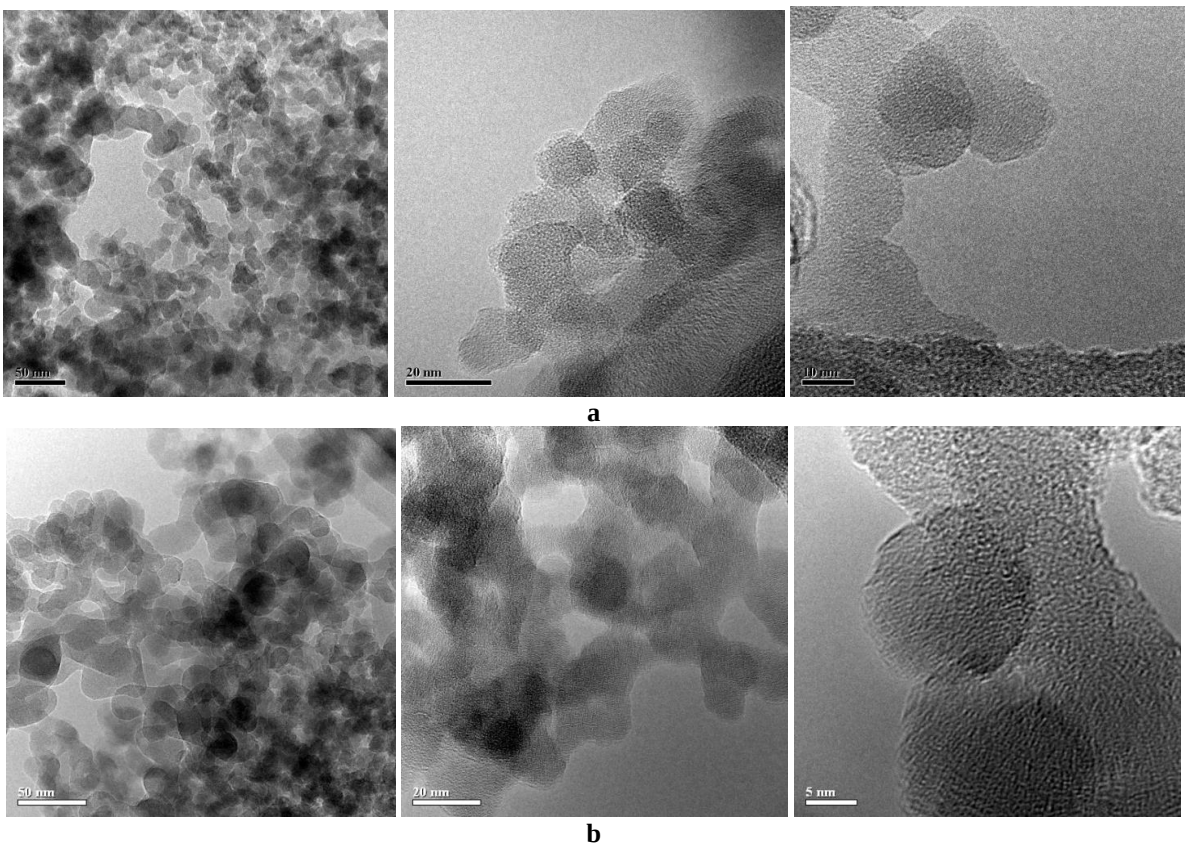

Fig. 2. TEM images of (a) A-150 and (b) A-380 samples morphology.

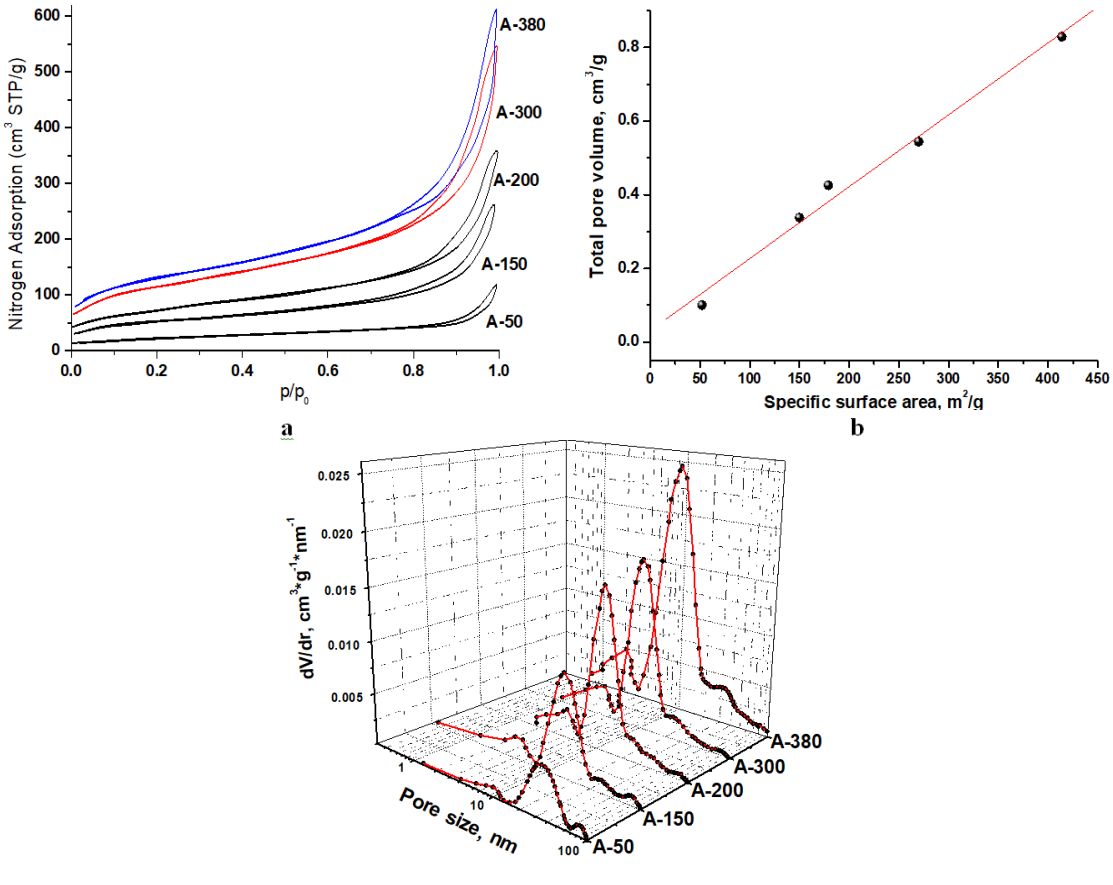

Fig. 3. (a) Nitrogen adsorption-desorption isotherms; (b) total pore volume vs. specific surface area, and (c) pore size distribution for fumed silica samples prepared at different synthesis conditions.

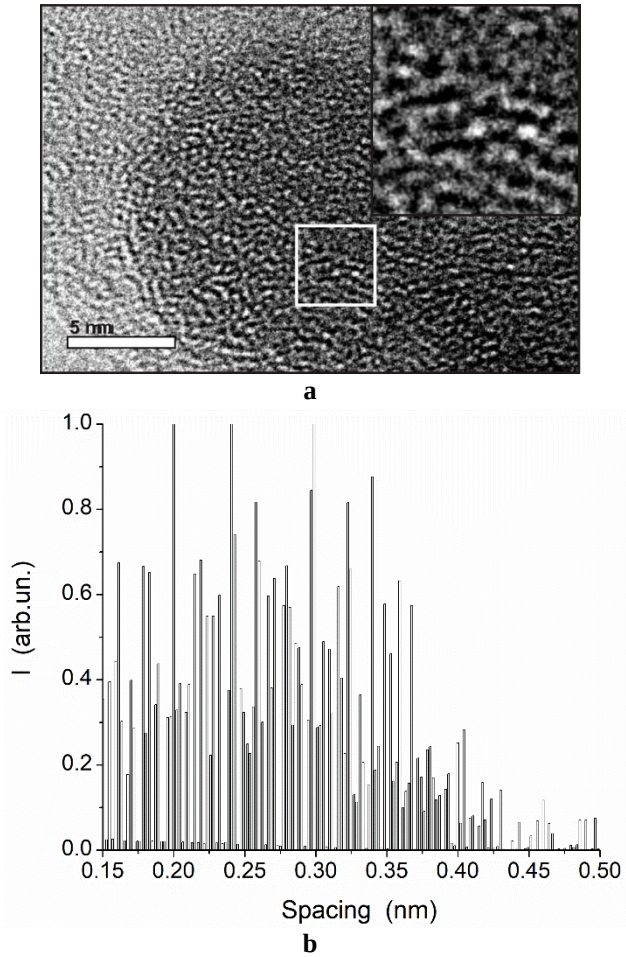

Fig. 4. (a) HRTEM image of fumed A-380 and (b) distribution spacing calculated using TEM image and Fiji/local thickness software (https://imagej.net/Fiji).

structural stability vs. tetrahedral coordination is ensured in the range of $0.225 < r_c/r_a < 0.414$. The silicon atoms typically have a tetrahedral coordination with r_c/r_a ratio close to 0.3. The [SiO_4] tetrahedra typically are bonded through common oxygen atoms without common edges. HRTEM image of fumed A-380 nanoparticles (Fig. 4) demonstrates filamentous domains (average length and width of about 0.6 - 2.4 and 0.26 - 0.28 nm, respectively). The average size of the [SiO_4] tetrahedra is 0.297 - 0.298 nm that is close to the observed domains width and the average height of the tetrahedron side, i.e., short filamentous domains formed by [SiO_4] tetrahedra. The similar linear clusters [$(SiO\text{-})_nO_2H_3$] were observed for porous silica prepared using the laser ablation method [19].

The linear condensation of the [SiO_4] tetrahedra during the pyrogenic synthesis causes the three-dimensional chains formation with nucleation of 3D silica particles on the next stage. This process is possible only with an open branched chain with a period of two tetrahedra (Fig. 5, a). The alternation period of the isolated chains is defined as the number of polyhedra in one repeating fragment of the linear part of the chain [20].

The formation of locally ordered three-dimensional structure is possible at the orientation of the [SiO_4] tetrahedra vertices perpendicular to the chains. In this case, the $\varphi_{Si\text{-}O\text{-}Si}$ angle along the linear chain is close to 180˚ and the formation of the six-chained rings upon [SiO_4] tetrahedra association is possible (Fig. 1, insert and 5, b). The atomic structure of amorphous SiO_2 is characterized by a series of oxygen atoms, the distance between which is equal to the length of the [SiO_4] tetrahedron edge (Fig. 4, b) surrounded by four groups of oxygen atoms. These groups of atoms in a plane perpendicular to the chain clusters are directly observed in HRTEM images. The three-dimensional atomic structure of fumed silica nanoparticles is formed by linear short and open clusters ordered with a period of two [SiO_4] tetrahedra. The spatial disorientation of chain clusters and their different lengths cause the long-range structural disordering of the fumed silica (Fig. 4, b). The confirmation of this hypothesis is possible with the careful analysis of FTIR data.

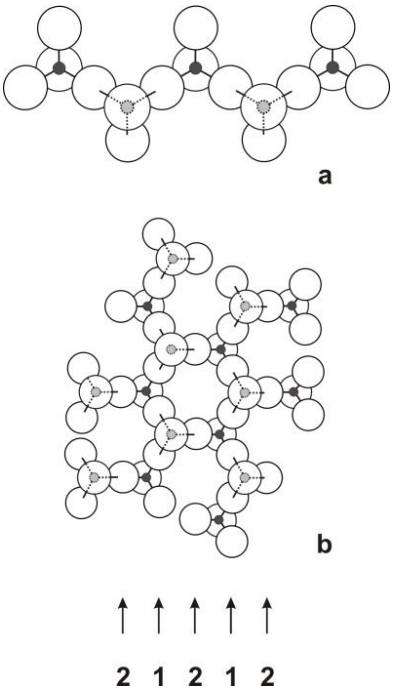

Fig. 5. The models of (a) linear [SiO_4] tetrahedra formed chain as a main structural unit of amorphous SiO_2 and (b) its possible arrangement in silica structure.

The typical infrared (IR) spectra of fumed silica nanoparticles are characterized by the presence of valence symmetric and asymmetric Si-O stretching vibrations in the [SiO_4] tetrahedra corresponding to bands at 808-810 cm^{-1} and 1300 - 900 cm^{-1}, respectively (Fig. 6, a). The band with a maximum at 480 - 471 cm^{-1} corresponds to the deformation vibrations of the siloxane framework.

The deconvolution procedure performed for wide bands at ca. 1400 – 900 cm^{-1} (Fig. 6, b) allows one to obtain additional information on structural ordering of silica samples. The analysis was realized using a specialized Univem 2.07 software. The spectral lines were fitted with pseudo-Voigt functions. The wide bands at a range of 1350 – 900 cm^{-1} was optimally decomposed with six spectral lines (Fig. 6, b).

The FTIR spectra of silica with the specific surface area of 52 $m^2 \cdot g^{-1}$ contain weak bands at ca. 1308 and

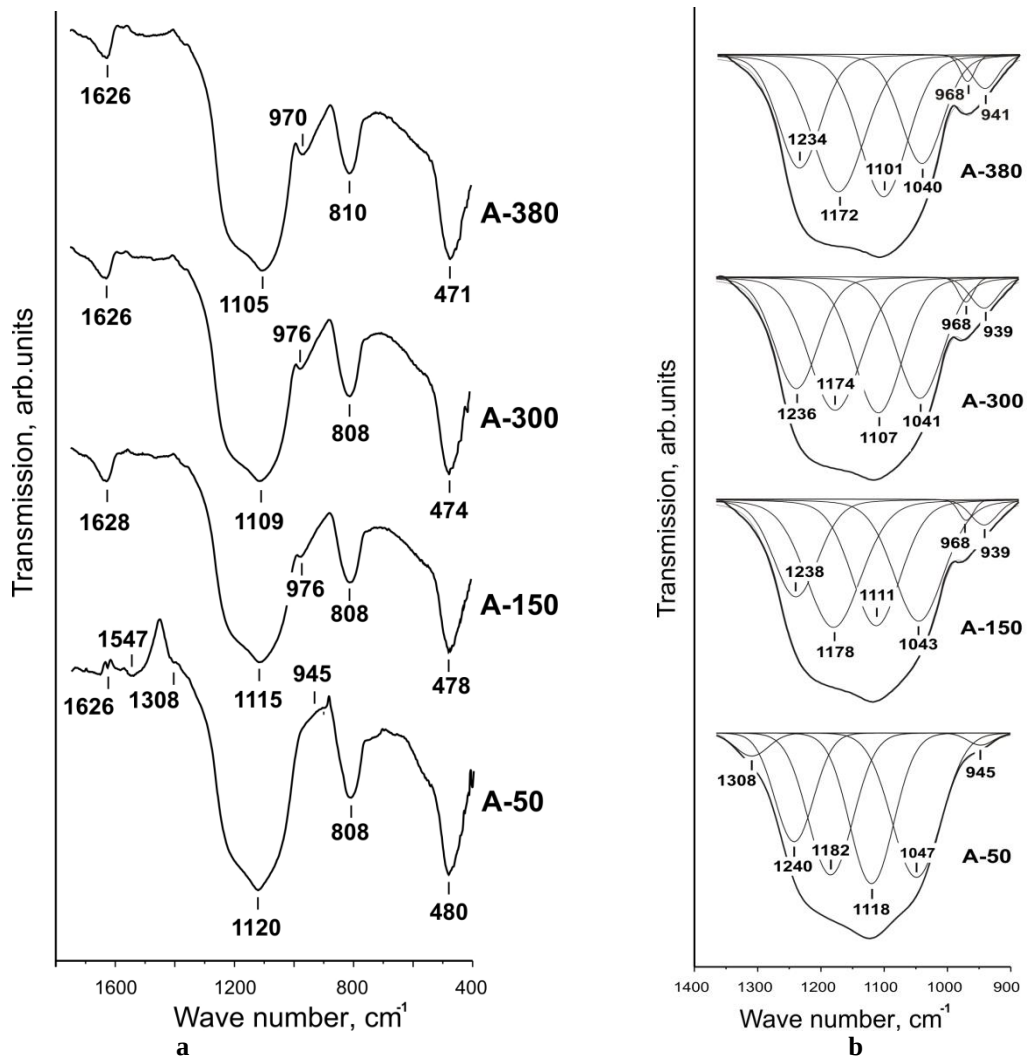

Fig. 6. (a) FTIR spectra of fumed silica samples and (b) the results of deconvolution of the bands at 1350-900 cm^{-1}.

945 cm^{-1}. A band at 1308 cm^{-1} is better observed with decreasing silica particle sizes. The band at 945 cm^{-1} growth and splits into two bands at ca. 968 and 939 - 941 cm^{-1} (Fig. 6, b). The intensity of four other bands at ca. 1240, 1182, 1118, and 1047 cm^{-1} decreases with decreasing average particle sizes. The observed longwave shift with decreasing nanoparticle sizes is a result of the size effect associated with the Laplace pressure influence [21].

The Si–O bond length and the φ_{SiOSi} angles for typical silicates vary in the range of $0.157\ nm < l_{Si-O} < 0.172\ nm$ and $120^\circ < \varphi_{SiOSi} < 180^\circ$ [20]. For crystalline silica modifications (quartz, cristobalite, coesite, and tridimite), the values of these parameters change in the ranges of $0.1594\ nm < l_{Si-O} < 0.1621\ nm$ and $137^\circ < \varphi_{SiOSi} \leq 180^\circ$. The peculiarity of the crystalline structure both of silica and silicates is the correlation between the siloxane bond lengths in the $[SiO_4]$ tetrahedra and the φ_{SiOSi} angle values. The increase in l_{Si-O} typically corresponds to the φ_{SiOSi} angle decreasing. The comparison of the structural characteristics of crystalline silica allows one to make a conclusion that only one of the four φ_{SiOSi} valence angles in coesite is equal to 180˚ when other is about 142 - 137˚. The corresponding Si – O bond length for the coesite is 0.1594 nm and 0.1621 nm. The differences in the atomic structure of crystalline silicas influence the FTIR spectra. The FTIR spectra of the typical crystalline modifications of silica (quartz, cristobalite, coesite, and tridymite) [22] were analyzed.

The IR spectra of coesite contain the characteristic bands at 1227 cm^{-1} and 1038 cm^{-1}. The asymmetric stretching vibrations frequency range for amorphous silica is respectively wider comparatively to crystalline silica spectra. The high-frequency band of asymmetric vibrations for fumed silica is observed at ca. 1240 - 1236 cm^{-1} (Fig. 6, b) that is an evidence of the shorter Si – O bonds and φ_{SiOSi} angle close to 180˚. The low intensity band of asymmetric vibrations at ca. 1038 cm^{-1} is characteristic of coesite only that the fumed silica contains the longer siloxane bonds compared to other silica modifications. The bands at ca. 1047 - 1040 cm^{-1} and 1182 – 1100 cm^{-1} indicate the presence the Si–O–Si bridges with the valence angles of ca. 137 - 147°. It is clear that the variations in the chain length and spatial ordering can cause a broader range of the valence angles in $[SiO_4]$ tetrahedrons in amorphous silica. At the initial stage of the pyrogenic synthesis, the interaction of $SiCl_4$

with water molecules leads to the formation of $Si(OH)_4$ orthosilicic acid. Their condensation in a turbulent reaction medium causes the formation of small SiO_2 protoparticles (nuclei). The growth of globules due to the coalescence of protoparticles is limited only by the flame temperature and reaction duration. During the molecules $Si(OH)_4$ condensation some silanol groups do not participate in the formation of three-dimensional structure. This is a reason of Si–OH bonds response in the FTIR spectra of fumed silica. The deformation vibrations of the O-H bonds in the silanol groups were detected as a band at 1628 - 1626 cm^{-1}. The band at 968 - 939 cm^{-1} in the spectra of small nanoparticles indicates the isolated chains formation with the edges connected $[SiO_4]$ structural units. There are two characteristic bands in the FTIR spectra of Si_2O_2-based clusters at ca. 950 - 980 and 1030 - 1050 cm^{-1} [23].

Conclusions

The atomic structure of fumed silica nanoparticles has been investigated using HRTEM, FTIR, quantum chemistry, and low-temperature nitrogen adsorption methods. It has been shown that fumed silica is characterized by short-range structural ordering. The X-ray amorphous silica is formed by linear open-branched chain clusters of ca. 0.6 - 2.4 nm in length. Each repeating fragment of a linear part of a chain cluster contains two $[SiO_4]$ tetrahedra bonded through a common oxygen atom. Inter-tetrahedral Si – O – Si angle along the chain is close to 180˚. The value of valence angles in Si – O – Si bridges between chains is about 137 - 147˚. The presence of small (< 10 nm) silica particles leads to the appearance of a weak band at ca. 968 - 939 cm^{-1} in the FTIR spectra that indicates the presence of $[SiO_4]$ tetrahedra with common edges. The textural porosity of fumed silica depends on the degree of aggregation of primary nanoparticles since the smaller the nanoparticles, the greater the porosity of the powder and the aggregation of NPNP. The mesopore volume in the fumed silica powder varies in the range of 0.26 - 0.60 $cm^3 \cdot g^{-1}$. The contribution of nanopores to the total pore volume is small as 0.003 - 0.030 $cm^3 \cdot g^{-1}$.

Mironyuk I.F. – Professor, Doctor of Chemical Sciences, Head of the Department of Chemistry;
Kotsyubynsky V.O. – Doctor of Physical and Mathematical Sciences, Professor of the Department of Materials Science and New Technologies;
Dmytrotsa T.V. – Assistant of Chemistry Department;
Soltys L.M. – PhD in Chemistry, Head of the Educational Laboratory of the Department of Chemistry;
Gun'ko V.M. – Professor, Doctor of Chemical Sciences, Head of the Department of Amorphous and Structurally Ordered Oxides.

[1] N.P. Bansal, R.H. Doremus, Handbook of glass properties (Elsevier, 2013).
[2] J.H. Konnert, P. d'Antonio, J. Karle, Journal of Non-Crystalline Solids 53(1-2), 135 (1982) (doi: 10.1016/0022-3093(82)90023-0).
[3] G.S. Smith, L.E. Alexander, Acta Crystallographica 16(6), 462 (1963) (doi: 10.1107/S0365110X63001298).
[4] Q. Ma, H. Fang, Z. Liu, S. Wang, Applied Thermal Engineering 131, 786 (2018) (doi: 10.1016/j.applthermaleng.2017.12.062).
[5] D. Hülsenberg, A. Harnisch, A. Bismarck, Microstructuring of glasses (Berlin: Springer) 87, 326 (2008).
[6] J. Fraissard, B. Imelik, J. Chim. Phys. et Phys. Chim. Biol. 59(4), 415 (2002).
[7] G.D. Chukin, A.I. Apretova, Journal of Applied spectroscopy 50(4), 418 (1989).
[8] G.E. Maciel, D.W. Sindorf, J. Amer. Chem. Soc. 102(25), 7606 (1980) (doi: 10.1021/ja00545a056).
[9] E. Lippmaa, M. Maegi, A. Samoson, G. Engelhardt, A.R. Grimmer, J. Amer. Chem. Soc. 102(15), 4889 (1980) (doi: 10.1021/ja00535a008).
[10] V.I. Zarko, V.M. Gun'ko, E. Chibowski, V.V. Dudnik, R. Leboda, Colloids and Surfaces A: Physicochemical and Engineering Aspects 127(1-3), 11 (1997) (doi: 10.1016/S0927-7757(97)00021-6).
[11] S.J. Gregg, K.S.W. Sing, Adsorption, Surface Area and Porosity, second ed. (Academic Press, London, 1982) (doi: 10.1002/bbpc.19820861019).
[12] V.M. Gun'ko, Applied Surface Sci. 307, 444 (2014) (doi: 10.1016/j.apsusc.2014.04.055).
[13] I.F. Myronyuk, B.M. Yaremchuk, T.V. Gergel, V.I. Mandzyuk, Physics and Chemistry of Solid State 7(4), 731 (2006).
[14] V.M. Gun'ko, V.I. Zarko, V.V. Turov, O.I. Oranska, E.V. Goncharuk, Y.M. Nychiporuk, E.M. Pakhlov, G.R. Yurchenko, R. Leboda, J. Skubiszewska-Zięba, V.D. Osovskii, Y.G. Ptushinskii, A.G. Derzhypolskyi, D.A. Melenevsky, J.P. Blitz, Powder Technol. 195, 245 (2009) (doi: 10.1016/j.powtec.2009.06.005).
[15] V.M. Gun'ko, V.V. Turov, E.M. Pakhlov, T.V. Krupska, B. Charmas, Appl. Surf. Sci. 459, 171 (2018) (doi: 10.1016/j.apsusc.2018.07.213).
[16] V.M. Gun'ko, Chemistry, Physics and Technology of Surface 10(4), 340 (2019) (doi: 10.15407/hftp10.04.340).
[17] L. Catoire, R. Mével, A. Kunz, P. Roth, Proceedings of the Combustion Institute 33(1), 477 (2011) (doi: 10.1016/j.proci.2010.05.009).
[18] V.D. Khavryuchenko, O.V. Khavryuchenko, V.V. Lisnyak, Critical Reviews in Solid State and Materials Sciences 36(2), 47 (2011) (doi: 10.1080/10408436.2011.572741).
[19] P.E. Lafargue, J.J Gaumet, J.F. Muller, A. Labrosse, J. Mass. Spectrom. 31(6), 623 (1996) (doi: 10.1002/(SICI)1096-9888(199606)31:6<623::AID-JMS333>3.0.CO;2-J).

[20] F. Liebau, Structural chemistry of silicates: structure, bonding, and classification (Springer Science & Business Media, 2012).
[21] V.M. Gun'ko, I.F. Mironyuk, V.I. Zarko, E.F. Voronin, V.V. Turov, E.M. Pakhlov, E.V. Goncharuk, Y.M. Nychiporuk, N.N. Vlasova, P.P. Gorbik, O.A. Mishchuk, A.A. Chuiko, T.V. Kulik, B.B. Palyanytsya, S.V. Pakhovchishin, J. Skubiszewska-Zięba, W. Janusz, A.V. Turov, R. Leboda, Journal of colloid and interface science 289(2), 427 (2005) (doi: 10.1016/j.jcis.2005.05.051).
[22] J.R. Michalski, M.D. Kraft, T. Diedrich, T.G. Sharp, P.R. Christensen, Geophys. Res. Lett. 30(19), PLA2-1–PLA2-4 (1997).
[23] D. Zhang, M. Zhao, R.Q. Zhang, J. Phys. Chem. B. 108(48), 18451 (2004) (doi: 10.1021/jp0469620).

І.Ф. Миронюк[1], В.О. Коцюбинський[1], Т.В. Дмитроца[2], Л.М. Солтис[1], В.М. Гунько[3]

Атомна структура та морфологія пірогенного кремнезему

[1]ДВНЗ «Прикарпатський національний університет імені Василя Стефаника», Івано-Франківськ, Україна, myrif555@gmail.com
[2]Івано-Франківський національний медичний університет, Івано-Франківськ, Україна, t0955386758@gmail.com
[3]Інститут хімії поверхні імені О.О. Чуйка НАНУ, Київ, Україна, vlad_gunko@ukr.net

У статті приведено порівняльний аналіз атомної структури і морфології пірогенних наночастинок кремнезему, які отрмані при різних умовах синтезу, за допомогою методів трансмісійної електронної мікроскопії (ТЕМ), ІЧ-спектроскопії та низькотемпературної адсорбції азоту. Визначено, що структура Х-променевоаморфного кремнезему формується відкриторозгалуженими ланцюжковими кластерами довжиною 0,6 - 2,4 нм. Лінійна частина цих кластерів складається з двох тетраедрів SiO_4 із спільним атомом оксигену та протилежно спрямованими вершинами. Міжтетраедричний середній кут зв'язків Si – O – Si становить приблизно 180˚. Показано, що пористість пірогенного кремнезему залежить від початкового ступеня агрегації наночастинок. Середній об'єм мезопор знаходиться в діапазоні 0,26 - 0,6 $см^3/г$ для матеріалів, які отримані за різних температур. Визначено, що середній розмір радіусу мезопор зменшується з 34 нм до 10 нм із зменшенням середнього розміру первинних наночастинок кремнезему. Вклад мікропор у загальний об'єм пор невеликий для всіх матеріалів (приблизно 0,003 - 0,029 $см^3/г$).

Ключові слова: пірогенний кремнезем, кристалічний кремнезем, кластери кремнезему, силоксановий зв'язок.